Large-Scale Flow Patterns and Their Influence on the Intensification Rates of Western North Pacific Tropical Storms*

JUSTIN D. VENTHAM AND BIN WANG

Department of Meteorology, University of Hawaii at Manoa, Honolulu, Hawaii

(Manuscript received 22 June 2005, in final form 19 June 2006)

ABSTRACT

NCEP–NCAR reanalysis data are used to identify large-scale environmental flow patterns around western North Pacific tropical storms with the goal of finding a signal for those most favorable for rapid intensification, based on the hypothesis that aspects of the horizontal flow influence tropical cyclone intensification at an early stage of development. Based on the finding that intensification rate is a strong function of initial intensity (Joint Typhoon Warning Center best track), very rapid, rapid, and slow 24-h intensification periods from a weak tropical storm stage (35 kt) are defined. By using composite analysis and scalar EOF analysis of the zonal wind around these subsets, a form of the lower-level (850 mb) combined monsoon confluence–shearline pattern is found to occur dominantly for the very rapid cases. Based on the strength of the signal, it may provide a new rapid intensification predictor for operational use. At 200 mb the importance of the location of the tropical storm under a region of flow splitting into the midlatitude westerlies to the north and the subequatorial trough to the south is identified as a common criterion for the onset of rapid intensification. Cases in which interactions with upper-level troughs occurred, prior to and during slow and rapid intensification, are studied and strong similarities to prior Atlantic studies are found.

1. Introduction

Tropical cyclones (TCs) at all stages of intensity are believed to be strongly influenced by variations in the vertical wind shear, in terms of their intensification and structure (DeMaria 1996; Bender 1997). It is generally accepted that variations in the horizontal characteristics of the environmental flow have an impact on the genesis process (Ritchie and Holland 1999). In the western North Pacific (WNP), Ritchie and Holland (1999), showed that five common lower-level large-scale flow patterns exist prior to and during genesis. The patterns all have cyclonic meridional shear of the large-scale zonal wind and/or confluence of the monsoon westerlies and trade easterlies. Confluence patterns were hypothesized to provide a favorable environment for genesis in terms of the production of mesoscale convective systems and their midlevel mesoscale vortices, eventually leading to genesis of a tropical depression. The confluence region also provides a favorable environment for the trapping of easterly waves and energy dispersed as Rossby waves from preexisting TCs. Shear line patterns were observed to have a slower in situ spinup of vorticity leading to genesis. Little attention in the literature has been paid to the possible continuing positive influence of the lower-level flow patterns on the intensification process. It has been argued that because of the high inertial stability of the mature TC core in the lower and midlevels, little or no direct low-level environmental influence on the core can occur. However tropical depressions and tropical storms (TSs) are commonly observed to have slowly decaying radial profiles of the tangential wind, and are thus not characterized by the high inertial stability typical of more intense systems (Mallen et al. 2005). Upper-level environmental forcing on TC intensity is known to be a factor, due partly to the much lower inertial stability of the weaker vortex there. Certain categories of upper-level flow patterns have been linked to be favorable for rapid intensification (RI) (Chen and Gray 1985). Specifically, the provision of several "outflow channels" was suggested

* School of Ocean and Earth Science and Technology Publication Number 6787 and the International Pacific Research Center Publication Number 388.

Corresponding author address: Justin Ventham, Department of Meteorology, University of Hawaii at Manoa, 2525 Correa Rd., Honolulu, HI 96822.
E-mail: ventham@hawaii.edu

DOI: 10.1175/MWR3327.1

to be more favorable. The purpose of this study is to examine the characteristics of the lower- and upper-level flow patterns around future RI TSs. We ask, is there a repeatable signal in the character of the flows that could be used for RI forecasts from the early stage?

The RI is poorly forecast and is a dangerous occurrence especially when it occurs near landfall. For example, the U.S. National Hurricane Center has 5% of 24-h intensity forecasts with errors exceeding 40 kt, mostly due to RI (Titley and Elsberry 2000). Mundell (1990) studied Joint Typhoon Warning Center (JTWC) intensity forecast errors and found that years with more RI cases had larger negative intensity forecast bias. Our lack of understanding of RI presents the possibility of large losses of life if evacuations are not performed based on a much lower-intensity forecast. The critical need for improved forecasts is predicting the few periods of RI, rather than the common slow change scenario. Section 2 contains a description of the data and methodology with close attention to how to define RI. It turns out that it makes most sense to define RI as a function of initial intensity. Section 3 contains the results in which the horizontal flow patterns around future RI TSs are examined and compared with a set of slowly intensifying (SI) cases. It is found that a strong lower-level combined confluence–horizontal shear pattern occurs predominantly for the most extreme RI cases. The character of upper-level trough–TS interactions are examined in section 4, prior to and during RI and compared to SI cases. The sequence of events, described by near superposition of an upper-level PV anomaly and the TS, appears very similar to the results of prior Atlantic-based studies. Section 5 contains discussions, conclusions, and avenues for further research.

2. Data and methodology

a. Definition of RI

In defining RI the JTWC best track is utilized, in which 6-hourly intensity and position data are supplied for the WNP from 1945 to 2001. A 24-h time period was chosen to highlight a sustained period of intensification and minimize short time-scale (<24 h) errors in intensity estimates.

Several prior studies have suggested definitions of RI. Holliday and Thompson (1979) gave a figure of 42 mb $(24\ \text{h})^{-1}$, representing the top 25% of *typhoon stage* intensifiers from 1956 to 1976, in the WNP. The Atlantic study of Kaplan and DeMaria (2003) gave a figure of 30 kt $(24\ \text{h})^{-1}$ representing the top 5% of intensity changers from 1989 to 2000. Their definition is based on all TCs 24-h intensity changes and is arrived at by including all *weakening and intensifying* systems in their cumulative frequency calculations. They also include all overlapping 24-h periods for every storm in their analysis and so do not pick out the onset of intensification clearly.

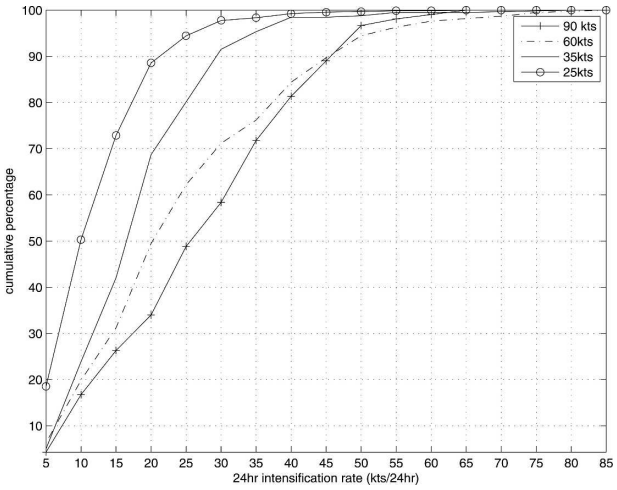

FIG. 1. Cumulative percentage distribution of 24-h intensification rates in the WNP (1975–2001), from initial intensities of 25, 35, 60, and 90 kt.

It became clear, from inspection of the JTWC best-track data, that for the purposes of this study, the definition of RI should take in to account both the initial intensity and onset time of intensification, rather than looking at overlapping time periods. Figure 1 shows the 1975–2001 distributions of 24-h intensification rates based on four different initial intensities (JTWC best track): 25, 35, 60, and 90 kt. Intensification is defined over a 24-h period, with the period *beginning with the criteria that in the first 6 h the system intensifies and does not weaken in the period.* These restrictions ensure that the cases counted are true 24-h intensifiers, showing no weakening trend within the period. The onset of intensification is also picked out consistently. If taking the 95th percentile for the definition of RI, the figures would be 30, 40, 55, and 55 kt from the aforementioned initial intensities, respectively. These are striking differences. As a further example of the differences, intensification rates up to and including 25 kt $(24\ \text{h})^{-1}$ account for 94%, 80%, 62%, and 48% of all intensifying cases from initial intensities of 25, 35, 60, and 90 kt, respectively. Intensification rate is a function of initial intensity with TSs able to intensify more rapidly than tropical depressions and early stage typhoons able to intensify more rapidly than weaker systems.

Kaplan and DeMaria (2003) did not define RI based on differing initial intensities. Figure 2 in Kaplan and DeMaria (2003) presents the cumulative frequency of 24-h intensity change rates for tropical depression, TS,

and hurricane stage in the Atlantic from 1989 to 2001. The 95th percentile is very similar for all these intensity ranges and is the basis of their choice of a figure of 30 kt (24 h)$^{-1}$. The similarity in the 95th percentile in 24-h intensity change for different intensity ranges is not because all stages intensify at similar rates, but because distributions of weakening cases are markedly different for the different intensity stages. Most notably weakening hurricane stage systems encompass 50% of all cases in this intensity range while weakening tropical depressions encompass only 10%. The combination of more common and rapid weakening and more common and faster intensification of hurricanes leads to the 95th percentile being similar to other initial intensity ranges. This masks the fact that the *intensification* rate distribution is different for the different initial intensities. They likely have hurricanes in their dataset that did not intensify rapidly if compared to others in that intensity range. An opposite argument would apply for tropical depressions, remarkable cases being omitted as not reaching their RI definition.

The distribution of intensification rates in the Atlantic (1989–2001), based on this study's definition are shown (Fig. 2). It can be seen that the initial intensity dependent intensification also occurs in the Atlantic. For initially 60- and 90-kt systems the 95th percentile would give a RI definition of ≥50 kt (24 h)$^{-1}$ and 55 kt (24 h)$^{-1}$, respectively, whereas for 25- and 35-kt systems the definition would be ≥35 kt (24 h)$^{-1}$ and 40 kt (24 h)$^{-1}$, respectively. It should be noted that the purpose of the Kaplan and DeMaria (2003) study was to estimate the probability of intensification of ≥30 kt (24 h)$^{-1}$ and for forecast applications this is a significant and potentially dangerous intensification rate from any initial intensity. For their purposes it is a consistent definition, but in the author's opinion future RI studies should take into account the obvious difference in intensification distributions based on initial intensities.

b. Storm sets

Taking into account the findings above and based on the hypothesis that *early* stage TCs may be more affected by the background environmental flow, a set of 88 TSs were identified from the JTWC best-track data (1975–2001). Each TS was chosen on the strict basis that it intensified by ≥30 kt in a 24-h period, initially from 35 kt (the earliest TS stage from JTWC best track). This rate represents the top 20% of intensifiers from *this initial intensity* (1975–2001; Fig. 1). As elucidated above, such an intensification rate is not remarkable for more intense storms and would be exceptional for weaker storms. There are 110 total cases. However,

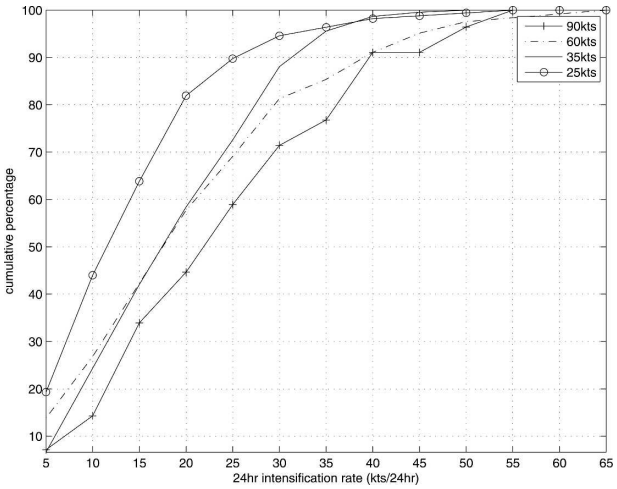

FIG. 2. Same as in Fig. 1 but for the Atlantic (1989–2001).

22 were removed after they experienced a period of weakening within the 24-h period, ensuring true 24-h intensifiers are considered. There is a large drop in the number of cases that intensify by ≥35 kt (24 h)$^{-1}$. Within the set are 19 cases that intensify very rapidly [i.e. very rapid intensification (VRI)] [≥40 kt (24 h)$^{-1}$], representing approximately the 95th percentile. Further subdivision of cases into a VRI subset yields interesting results. For comparison a set of 58 cases with an SI [10 kt (24 h)$^{-1}$] from an initial intensity of 35 kt is included. This set was chosen using the same specifications (no weakening within the 24-h period and intensification in the first 6-h subperiod) as for the RI cases.

c. Analysis fields

The National Centers for Environmental Prediction–National Center for Atmospheric Research (NCEP–NCAR) reanalysis (2.5° resolution) horizontal wind components are retrieved for the time just prior to the onset of intensification (t_0: the time when the system is 35 kt and intensifies in the next 6-h period) and are utilized to define circulation patterns around cases at 850 and 200 mb. Temperature data are also included, allowing the calculation of potential vorticity. All fields are storm centered on 60° latitude × 90° longitude grids, suitable for composite analysis. The storm centers were identified by visually inspecting the NCEP–NCAR wind fields for the streamline circulation center and maximum vorticity at 850 mb. The JTWC reported positions were used as guide, but the NCEP–NCAR data were used for the final grid placement of all TSs. There was a high degree of agreement between JTWC best-track positions and NCEP–NCAR-derived positions. Differences never exceeded 1 grid point (~250 km).

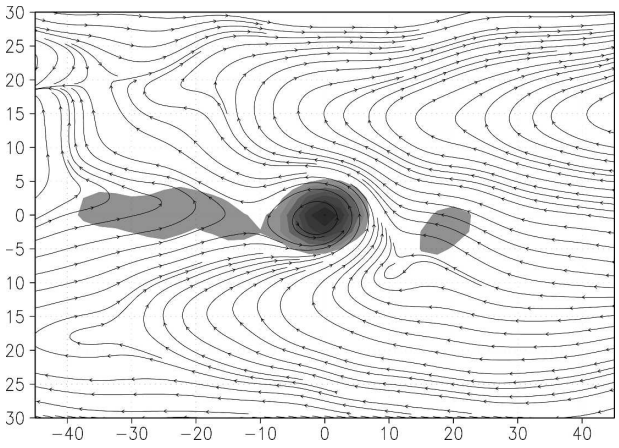

FIG. 3. Composite 850-mb streamlines and vorticity (shaded values $>2 \times 10^{-5}$ s^{-1}, interval 0.5×10^{-5} s^{-1}) for 88 cases of RI from 35-kt initial intensity. The x axis is the storm's relative longitude and the y axis is the storm's relative latitude.

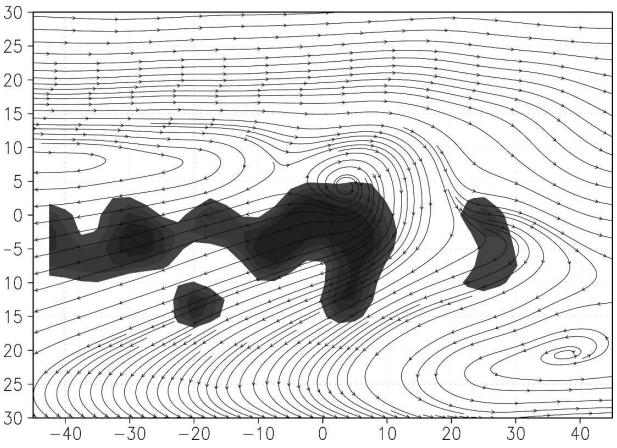

FIG. 4. Same as in Fig. 3, but for 200-mb streamlines and divergence (shaded values $>2 \times 10^{-6}$ s^{-1}, interval 0.5×10^{-6} s^{-1}).

d. Identification of common flow patterns

The WNP (5°–30°N, 100°E–180°) flow patterns change markedly by season, being characterized by a winter trade wind regime to the summer monsoon (Sadler 1975). The summer monsoon begins between April and May and in the peak phase (July–October) is often characterized by a band of westerlies with cross-equatorial flow meeting the central Pacific trade winds. Winter trade flow returns in December. The peak in TC activity occurs in the monsoon season with the presence of the monsoon trough leading to enhanced conditions for genesis (Ritchie and Holland 1999). The approach of this work is to visually compare the total composite wind fields at 850 and 200 mb just prior to RI and SI and then use a statistical approach to identify and subdivide the common large-scale flow patterns around RI cases. Scalar empirical orthogonal function (EOF) analysis of the anomaly fields for the zonal component of the wind at 850 mb is performed on the *storm-centered grids*.

As a basis for the description of large-scale circulation variability around the TS cases, the spatial EOF method defines a small set of recurrent patterns (EOFs) that describe the intrinsic structure of the variability within the dataset. The patterns are orthogonal and arranged in decreasing order according to how much variance in the dataset they explain. The relative importance or partition of the variance for any one of the cases is defined by the principal components (PCs) that are associated with each EOF. The time series of a principal component for an EOF describes how closely a case corresponds to a particular spatial pattern (EOF). In this way storms may be subdivided into composites according to how large a particular PC is for its associated EOF. According to the orthogonality condition of the EOFs, distinctly different circulation patterns are defined. More details of the technique may be found in Peak et al. (1986). Care must be taken that the method picks out physical flow patterns.

3. Results

a. Total composites

To gain an overall appreciation of features common to the 88 cases of RI, all t_0 cases are composited. This method has the advantage of picking out features common to many cases but smoothes out potentially important variability between cases. Figures 3 and 4 show the 850 and 200 mb, t_0 RI total composite wind fields with values of vorticity and divergence shaded. Figure 3 reveals a composite TS and its associated vorticity maximum at the center of the grid with cross-equatorial flow to the south, curving into monsoon westerlies, meeting trade easterlies just to the east of the TS. The composite equator may be identified by the point at which the flow to the south of the TS curves from an easterly to westerly component (about 15°S of the TS). The composite TS is located on the eastern extremity of a zonally extensive region of cyclonic vorticity, associated with the monsoon trough. The subtropical ridge lies about 15° to the northeast of the composite TS. The flow pattern is characterized by cyclonic meridional shear of the zonal wind (easterlies to the north of the TS and westerlies to the south), and by easterlies meeting westerlies just to the east of the TS.

A 200-mb anticyclonic center is located about 400 km to the northeast of the lower-level TS with northeasterly divergent flow to the south flowing into the sub-

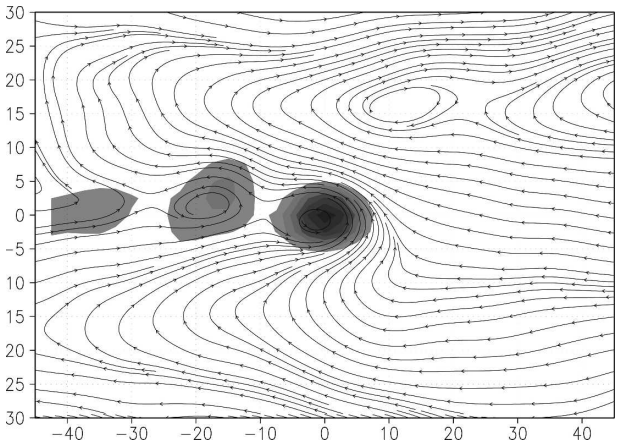

FIG. 5. Same as in Fig. 3, but for 850-mb streamlines and vorticity (shaded values $> 2 \times 10^{-5}$ s^{-1}, interval 0.5×10^{-5} s^{-1}) for 58 cases of SI.

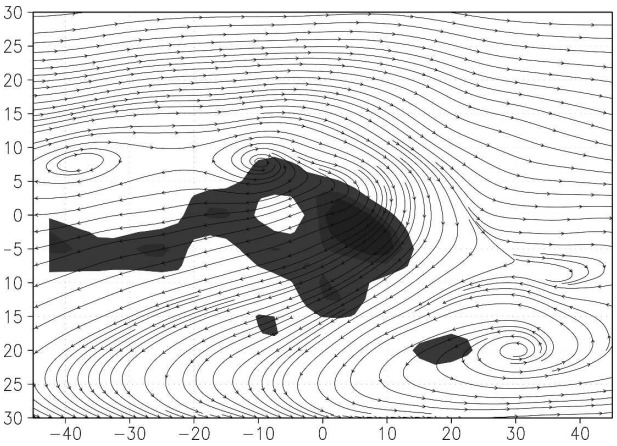

FIG. 6. Same as in Fig. 3, but for 200-mb streamlines and divergence (shaded values $> 2 \times 10^{-6}$ s^{-1}, interval 0.5×10^{-6} s^{-1}) for 58 cases of SI.

equatorial trough and southerly flow just to the north (Fig. 4). The upper-level subtropical ridge extends zonally to the west of the domain, about 5°N of the composite TS. A composite tropical upper-tropospheric trough (TUTT) is located to the northeast of the domain, a common feature of the WNP flow during summer (Sadler 1975). The TUTT was hypothesized by Ritchie and Holland (1999) to be attendant to the lower-level confluence pattern, providing a possible enhancement to this lower-level pattern by increasing downward motion at lower levels and enhancing the subtropical high and its trade winds below. The location of the anticyclonic center (which is probably the merged result of the upper-level subtropical high and the TC associated outflow anticyclone at this low resolution) puts the lower-level TS very close to a region of flow splitting to the north and south, aiding outflow to the north and south. However, if one follows the streamlines close to the TC center, they all go into the Southern Hemisphere. On examination of individual cases, many have streamlines that do connect with the midlatitude westerlies to the north. The compositing technique smears this feature out. As will be shown, the upper-level field for the SI cases shows no hint for unrestricted outflow to the north and is markedly different from the RI field. The condition of several outflow avenues has been previously linked as more favorable for more RI than for cases in which just the usual channel to the south is available (Chen and Gray 1985). The upper-level TUTT to the northeast of the TS produces a band of westerly flow 20° to the east. So in addition to the equatorward and poleward composite outflow there is flow extending far eastward, south of the TUTT. However, the connection to the TC outflow is unclear in the composite sense of this study. The work of Spratt (1990) noticed that eastward-orientated cloud patterns were often associated with the most rapid intensification rates south of the TUTT after examining several years of satellite pictures.

b. Slow intensification composites

Figures 5 and 6 give the composite 850- and 200-mb patterns, respectively, for the 58 SI cases. At 850 mb the SI composite wind field (Fig. 5) appears very similar to the RI counterpart (Fig. 3). The main features described previously appear in both SI and RI composites.

There is a striking difference between the RI 200-mb composite (Fig. 4) and the SI 200-mb composite (Fig. 6). The composite SI TS is located below northeasterly flow. The flow splitting the north is not evident for the SI cases, thus outflow is unrestricted only to the south. The upper-level anticyclonic center is located about 1000 km to the northwest. Since we are discussing composites of 88 and 58 cases the composite analysis gives confidence in the robustness of the difference. Also, the TS outflow certainly cannot be seen to join flow to the south of the TUTT in an eastward-extension pattern.

c. Composite comparisons

It proves useful to further subdivide the RI cases into 19 VRI cases that intensify by $\geq$40 kt (24 h)$^{-1}$ and 69 "regular" RI cases. To test for statistical differences between the three composite subsets, a simple two-sided *t* test is performed in which we test for a significant difference in the means of the wind components for the three subsets over the analysis domain.

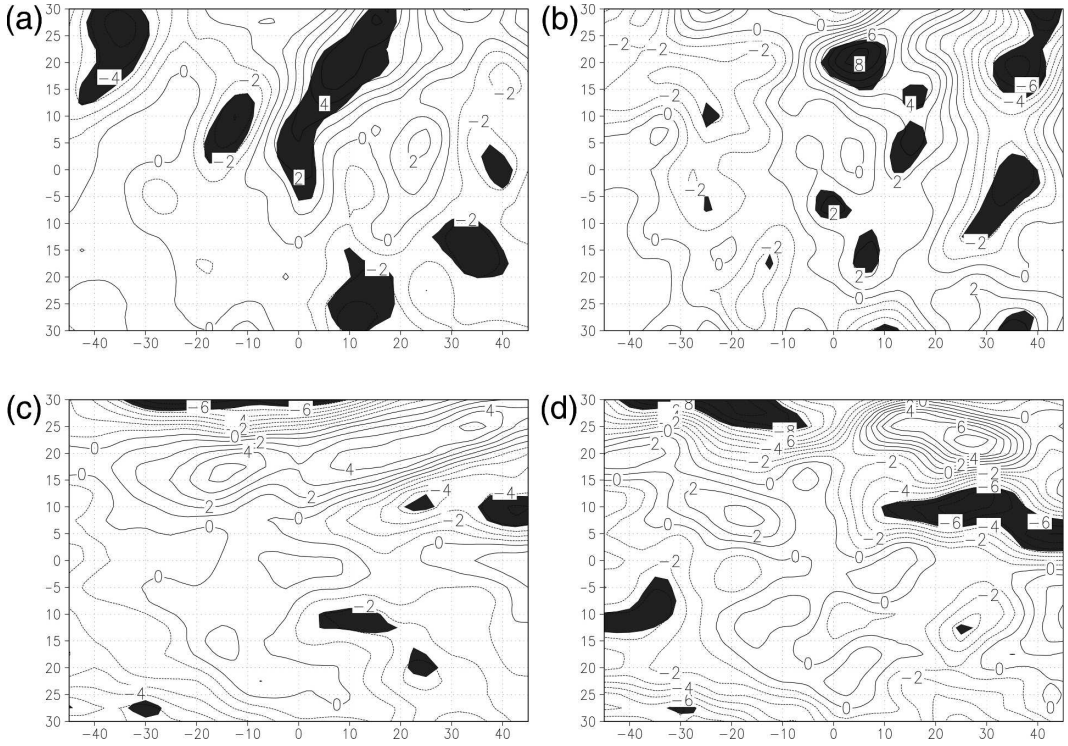

FIG. 7. (a) The RI 200-mb composite meridional wind ($m\,s^{-1}$) minus SI 200-mb composite meridional wind. Shaded areas show where difference is significant to 95% and beyond. (b) Same as (a), but for VRIs minus SIs. (c) Same as (a), but for zonal wind component. (d) Same as (b), but for zonal wind component. The *x* axis is the storm's relative longitude and the *y* axis is the storm's relative latitude.

The test is first applied to the 200-mb wind components. Figures 7a,b show the result of subtracting the SI from the RI composite meridional wind and the SI from the VRI composite meridional wind, respectively. The shaded zones show where the difference is significant to the 5% level as determined by the *t* test. Southerlies to the north and northerlies about 1000 km to the northwest are significantly stronger for the RI subset than the SI subset. This is an indication that the difference in the placement of the upper-level anticyclonic centers is robust. The VRI cases have a stronger southerly component to the north of the TS and a stronger northerly component to the east than for SI (Fig. 7b). The zonal differences for the VRI and SI subsets (Fig. 7d), shows a significantly stronger easterly component over 1000 km to the northeast of the TS center (with stronger westerlies to the south of this area). This reveals the existence of a statistically stronger cyclonic circulation to the east for VRI cases. The anomalous easterly zone is a result of weakened westerly flow in this area, due to the presence of the stronger TUTT. A similar but less strong result can be deduced from comparison of RI and SI cases (Fig. 7c). In summary robust differences deduced between the three subsets at 200 mb are the following:

1) RI cases have a stronger TUTT-like circulation to the east than SI,
2) VRI cases have a signal for a stronger TUTT circulation to the east as compared to other subsets, and
3) RI cases are situated such that the upper-level anticyclone is just to the northeast whereas the main anticyclonic center is located over 1000 km to the west for SI.

The 850-mb test shows that there are virtually no significant differences within 1000 km of the TS between the RI and SI composites for meridional or zonal winds (Figs. 8a,c). When comparing 19 VRI and 58 SI cases, a distinct difference in the 850-mb fields appears. Figure 8b shows the composite meridional wind component of the 19 VRI cases minus the 58 SI cases. The VRI cases have a large area of significantly stronger southerlies in a north–south-orientated band several thousand kilometers from the TS. Comparing this result to the test between VRI and SI zonal components (Fig. 8d), an area of stronger easterlies can be matched to the southern portion of the VRI strong southerlies. That is the trade winds associated with the subtropical high are stronger. The VRI cases also have a large area of significantly stronger westerlies to the southwest of

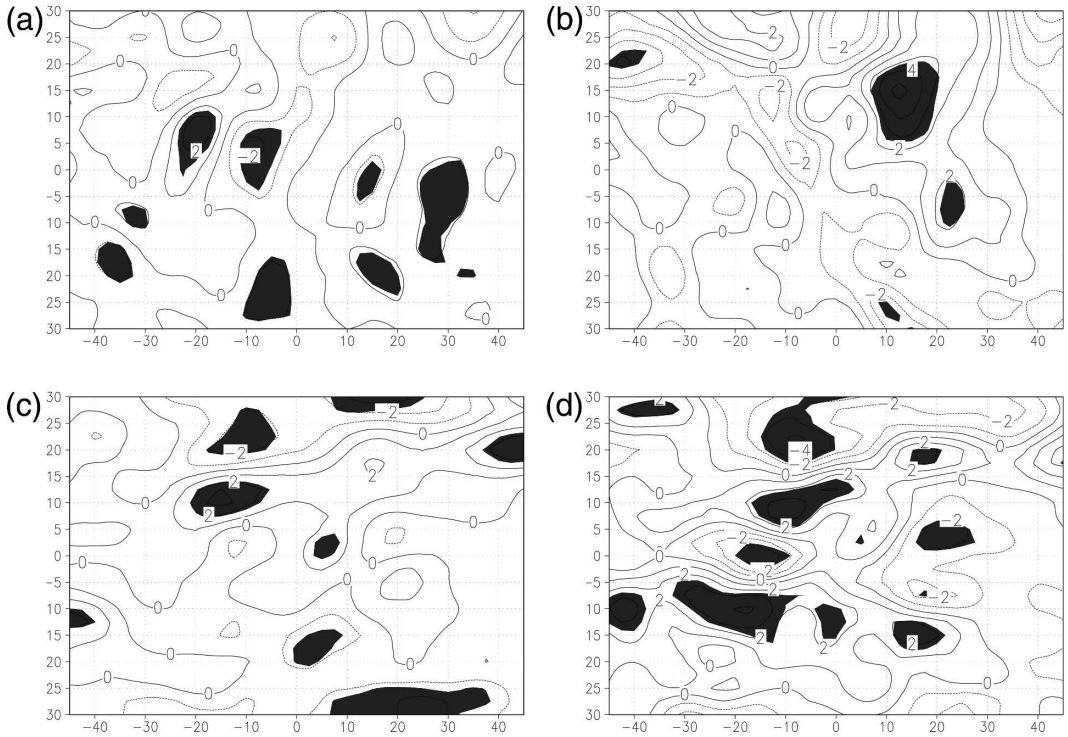

FIG. 8. Same as in Fig. 7, but at 850 mb.

the domain (up to 3 m s^{-1} stronger than the SI composite). The interpretation of this result is that for the VRI cases, the confluence of a region of westerlies meeting easterlies just to the east of the composite TS is stronger than for the SI cases. If the regular RI cases are compared in the same way with the VRI cases, a similar but less strong result is found (not shown).

The lower-level confluence and upper-level TUTT circulations appear to increase in strength together for RI and VRI cases as compared to SI cases. This makes it difficult to speculate on the real instigator of RI and VRI. The placement of an upper-level TUTT system to the east could provide an eastward extension of the TS outflow, improving the likelihood of RI and also enhancing the confluence region below by strengthening the lower-level subtropical high, its trade winds, and therefore the attendant confluence zone. The lower-level composite of the RI and SI cases has characteristics of several circulation patterns described in Ritchie and Holland (1999), suggesting subdivision of the composite may yield several distinct circulation patterns and better clarify these results.

d. Subdivision of the composites

To effectively subdivide the cases, scalar EOF analysis was performed on the anomaly zonal component of the wind at 850 mb, for the 88 RI cases. Anomaly zonal component refers to the fact that the EOF analysis was performed on the 88 cases with the mean at each grid point removed. The composite analysis and tests for statistical differences between RI, VRI, and SI storm sets found that a signal emerges for a significant difference between VRI cases and the other subsets. VRI distinguishes itself from "regular RI." There was little difference overall between the regular RI and SI wind circulation patterns at 850 mb. Therefore EOF analysis is applied to all 88 RI cases with the primary goal of finding a VRI pattern that may distinguish itself from regular RI.

Four different zonal wind patterns (EOF1, EOF2, EOF3, and EOF4) were found that account for 14%, 11%, 7%, and 6% of the total variance, respectively (Figs. 9a–d). The method used for deciding which eigenvectors to keep is that of North at el. (1982). This simple yet powerful tool recognizes that if two neighboring eigenvalues are too close in magnitude, then there is likely serious contamination between neighboring EOFs and the physical interpretation of the patterns is impeded. The first four EOFs satisfy North's rule of thumb and as will be discussed may be physically interpreted. Figures 10a–d show the associated anomaly composite of the actual data, where the EOF1–4-associated PC is greater than one standard de-

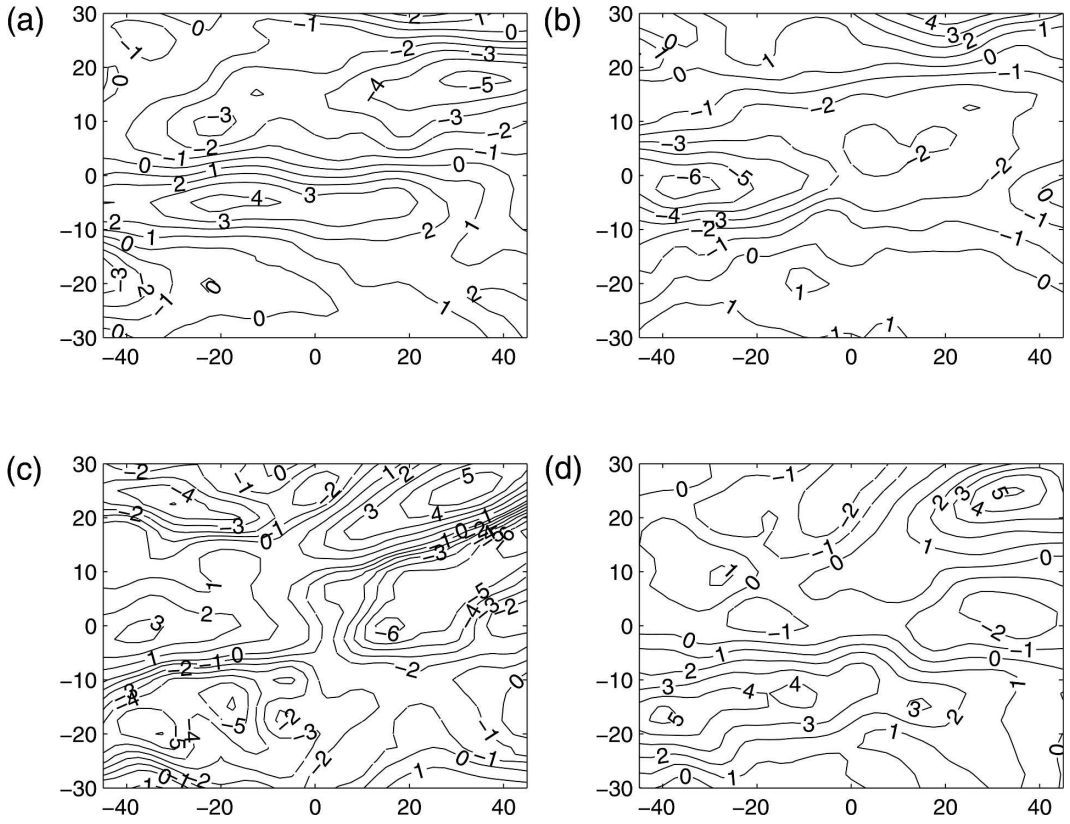

FIG. 9. (a) EOF1 of anomaly zonal wind ($m\ s^{-1}$) for 88 rapid intensifiers (14% of variance), (b) EOF2 (11% of variance), (c) EOF3 (7% of variance), and (d) EOF (6% of variance).

viation above the series mean. Cases that had more than one EOF with a PC with its magnitude more than 1 standard deviation above its series mean were subdivided according to the case with the largest eigenvalue. There were only five cases that had to be treated in this manner, suggesting a clear difference in the EOF1–4 patterns. Because the composites include only analyses that have large principal component, they are considered to be characteristic of the variability in the anomalous circulation patterns. In all four cases the EOF strongly resembles the actual anomaly composite, giving confidence that the method picks out realistic physical modes.

e. Description of EOFs

All of the anomaly patterns describe a distinct zonal wind configuration. Figures 11a–d give the actual composite circulation patterns corresponding to the EOF1–4 patterns. Figures 12a–d present the 200-mb composite wind fields corresponding to the 850-mb EOFs and Figs. 13a–d show the tracks of the cases.

EOF1 (Fig. 9a) is characterized by anomalous easterlies to the north of the TS and anomalous westerlies to the south, both of which extend zonally across the grid. The corresponding composite circulation pattern (Fig. 11a) resembles a monsoon shear line (Ritchie and Holland 1999) and what this study will term as an anomalous monsoon shear line. This pattern often occurs in the late season, 8 of 15 cases occur in October–December (OND) and has an average position of (11.5°N, 138°E; Fig. 13a). The composite TS is located within an anomalously strong region of cyclonic meridional shear of the zonal wind. About 20° to the east is the monsoon confluence region where easterly trade flow meets monsoon westerlies. About 20° to the west of the TS is another vorticity maximum, which on examination of individual cases corresponds to the presence of another TC within the monsoon trough. Eleven of the 15 cases that make this composite have a TC within 25° to the west.

EOF2 (Fig. 9b) is a pattern with anomalous easterlies extending zonally across the grid with their maxima near the western edge of the domain. Anomalous westerlies appear at the far north of the grid and in the southern 20° portion of the grid. Physically the pattern depicts a TS in easterly flow (Fig. 11b), to the south of a zonally orientated subtropical ridge extending longitudinally across the domain. This pattern is a late-sea-

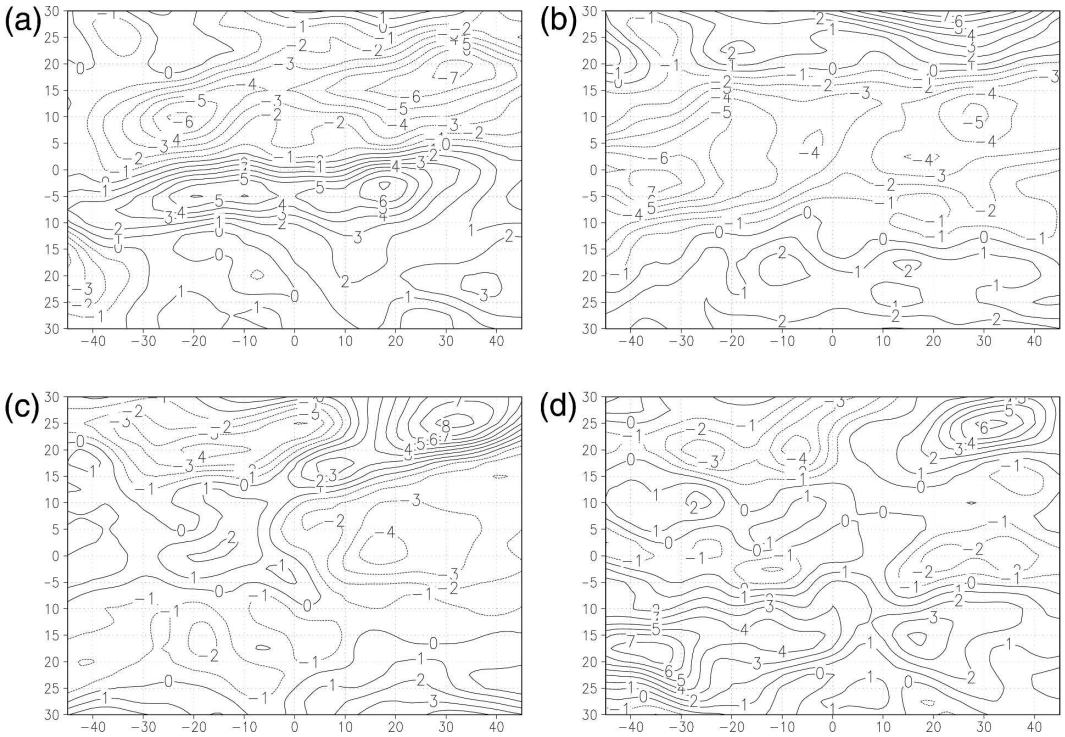

FIG. 10. (a) Composite of anomaly zonal wind ($m\ s^{-1}$) for all RIs where the PC is greater than one standard deviation above its own series mean. (b) Same as in (a), but for PC 2. (c) Same as in (a), but for PC 3. (d) Same as in (a), but for PC 4. The *x* axis is the storm's relative longitude and the *y* axis is the storm's relative latitude.

son scenario, with 13 of 15 cases occurring in OND, and it occurs at an average position of 11°N, 140°E (Fig. 13b).

EOF3 (Fig. 9c) is characterized by an anomalously strong subtropical high to the northeast of the domain (anomalous easterlies to its south and anomalous westerlies to its north). Fourteen cases make this composite. At the latitude of the TS, anomalous westerlies to the west meet anomalous easterlies to the east. Figure 11c depicts a composite TS at the eastern edge of a zonally orientated region of positive vorticity (monsoon trough). A long run of easterly trades meets monsoon westerlies in the monsoon confluence region with the TS located on the cyclonic shear side of the monsoon circulation. This pattern occurs at an average position of 13°N, 140°E in June–December but on average some 20° to the west in the earliest month (Fig. 13c).

EOF4 (11 cases) like EOF3 has an anomalous anticyclonic region to the northeast of the domain (Fig. 9d) but differs in that anomalous westerlies occur to the southwest of the TS center. The physical wind pattern (Fig. 11d) may also be described as a monsoon confluence region but is different from that described by EOF3. The pattern occurs June–December, but in contrast to EOF3, occurs to the northwest of the domain at an average position of 19°N, 128°E (Fig. 13d). Two late-season cases occur at the low latitude of 10°N. Strong anomalous westerlies cover a larger area meridionally to the southwest of the composite TS and the circulation of the TS appears larger than the EOF3 case. Anomalous easterlies exist to the north of the TS over much of the zonal domain. The pattern should therefore be described as a "hybrid pattern," in which the meridional cyclonic shear and confluence characteristics of the flow are stronger than usual, as compared to other RI cases.

The 200-mb composites have some remarkable consistencies (Figs. 12a–d). The EOF1 200-mb pattern (Fig. 12a) has weakly divergent easterly flow above the low-level composite TS with stronger divergent flow to the south. The strongest divergent flow lies southwest of the composite TS with the axis of the subtropical ridge about 10° to the north. Overlying the composite confluence region (identified in the 850-mb field) is a secondary region of maximum divergence. The EOF2 200-mb pattern (Fig. 12b) has an anticyclonic center, centered about 700 km to the northeast of the composite TS with maximum divergent flow to the north and south of the composite TS. The flow splits just north of

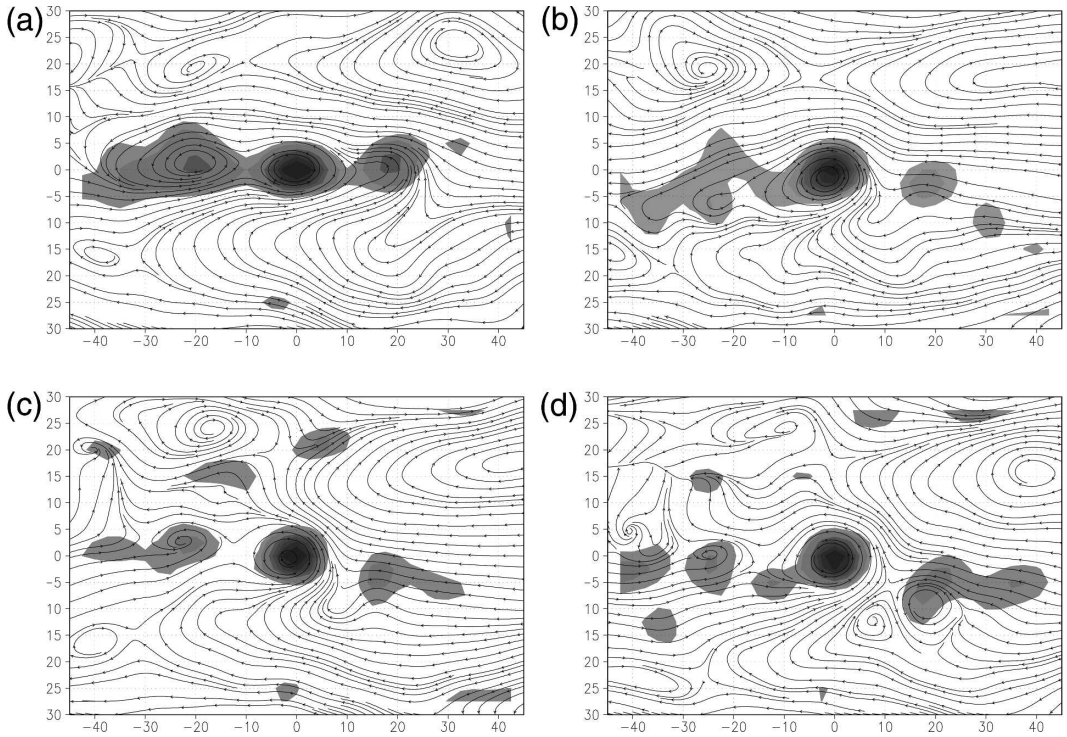

FIG. 11. Composite wind field and vorticity (s^{-1}) at 850 mb (shaded for values $>2.5 \times 10^{-05}$ s^{-1}, interval 0.5×10^{-5} s^{-1}) for (a) PC 1 greater than one std dev above its own series mean. (b) Same as in (a), but for PC 2. (c) Same as in (a), but for PC 3. (d) Same as in (a), but for PC 4. The *x* axis is the storm's relative longitude and the *y* axis is the storm's relative latitude.

the TS with southerly flow joining the midlatitude westerlies and easterly flow to the south with a cross-equatorial component. As is the case for the EOF1 200-mb pattern, a secondary region of divergence lies to the east of the TS center. The EOF3 200-mb pattern (Fig. 12c) has an anticyclonic center to the northeast with maximum upper-level divergence to the southwest. An area of cyclonically curved streamlines to the northeast is in the position of a composite upper-level trough (TUTT). The EOF4 200-mb pattern (Fig. 12d) is characterized by an upper-level anticyclonic vorticity maximum in a position very close to that of EOF2 and EOF3. Maximum divergence lies over and to the southwest of the TS center with divergent westerly flow also to the north.

A common characteristic of the upper-level composites for EOF2, EOF3, and EOF4 is the location of the upper-level high center just to the northeast of the lower-level TS. This configuration results in very light total vertical wind shear (<2 m s^{-1}) over the composite TS (not shown) as well as assisting outflow to the north (into the midlatitude westerlies) and to the south. An upper-level TUTT appears in all of the composites to the northeast. The TUTT is most evident for EOF3 and EOF4, the confluence and combined horizontal shear/confluence patterns.

f. Very rapid intensification and EOF patterns

There are 19 VRI cases that intensify by ≥40 kt (24 h)$^{-1}$. By inspecting the associated PCs for these cases it was noticed that 14 of 19 cases have PC3 or PC4 as the largest PC. All of these cases have PC3 or PC4 magnitude greater than 0.75 standard deviations above the series mean. Nine of the 19 cases have PC4 largest with an average magnitude of 1.10 standard deviations above the series mean. The large magnitude of PC4 for the VRI cases was found to be statistically significant as compared to the rest of the RI sample to beyond the 5% level based on a Student's *t* test. Both EOF3 and EOF4 describe variations of the confluence patterns. Since EOF1 and EOF2 (accounting for 14% and 11% of the variance) represent more dominant modes than EOF3 and EOF4 (accounting for 7% and 6% of the variance) it is interesting to note that for the VRI cases, EOF3 and especially EOF4 appear as the dominant modes in terms of the magnitude of their PCs. Figure 14 is a composite of the anomalous 850-mb zonal wind component for all 19 VRI cases (anomalous with re-

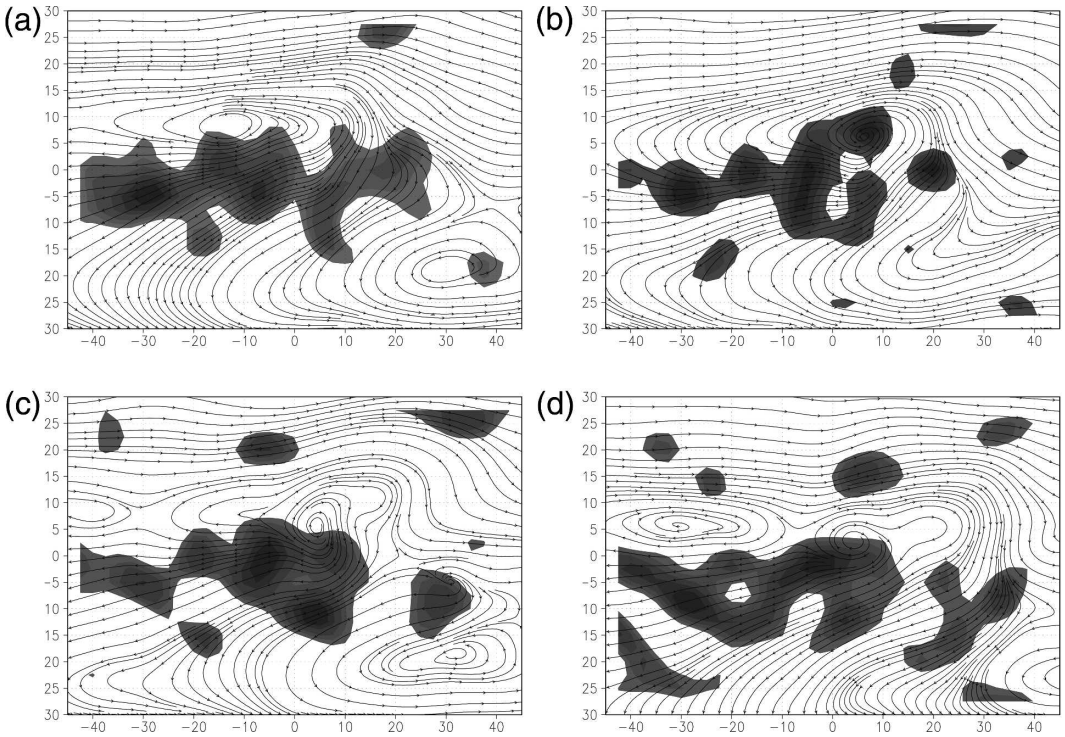

FIG. 12. Composite wind field and divergence (s^{-1}) at 200 mb (shaded for values $>2 \times 10^{-6}$ s^{-1}, interval 0.5×10^{-6} s^{-1}) for (a) PC 1 greater than 1 std dev above its own series mean. (b) Same as in (a), but for PC 2. (c) Same as in (a), but for PC 3. (d) Same as in (a), but for PC 4. The *x* axis is the storm's relative longitude and the *y* axis is the storm's relative latitude.

spect to all 88 RI cases). It can be seen that the anomaly composite resembles EOF4 strongly (see Fig. 10d). The main difference is that the main band of anomalous westerlies, to the southwest of the TS, are 5° farther north than that of the pure EOF4 composite. This is reflection of the five cases that resemble EOF3 more strongly. These results suggest that the VRI cases are preferentially associated with strong confluence or combined horizontal shear–confluence patterns at the lower levels (as was also suggested by the composite analysis), as opposed to the more common pure shear line and easterly flow patterns. The anomalous confluence patterns, EOF3 and EOF4, also have stronger 200-mb TUTTs to the northeast, further suggesting that the two systems are coupled.

g. Stability of EOF patterns

Although the four EOFs are explainable as physical *large-scale* flow patterns, it is possible that the large-scale interpretation could be compromised by other randomly positioned TCs within the dataset. The dataset was randomly divided into two parts and the EOFs were rederived for the two subsets and the experiment was repeated multiple times. The four EOF patterns for different subdivisions were very similar suggesting the patterns are truly large scale and not sensitive to other vortical disturbances (significant smaller-scale anomalies) within the domain. Higher-order modes (EOF5 and beyond) were highly sensitive to the subdivisions. The higher-order EOFs (not shown) are much more complex as a result of these modes being a reflection of both data noise and the smaller-scale flow variations produced by the random spatial distribution of other TCs within the dataset

There are nine cases that do not have any of PC1–4 large and dominant. Visual inspection of these cases revealed highly complex flow patterns including multiple TCs. It was difficult to ascribe a large-scale flow pattern to these cases.

4. Upper-level trough interactions prior to and during TS intensification

A set of storms intensified after the approach of an upper-level vorticity maximum. The trailing edge of an upper-level midlatitude trough, or more commonly an upper-level TUTT cell circulation approached within a

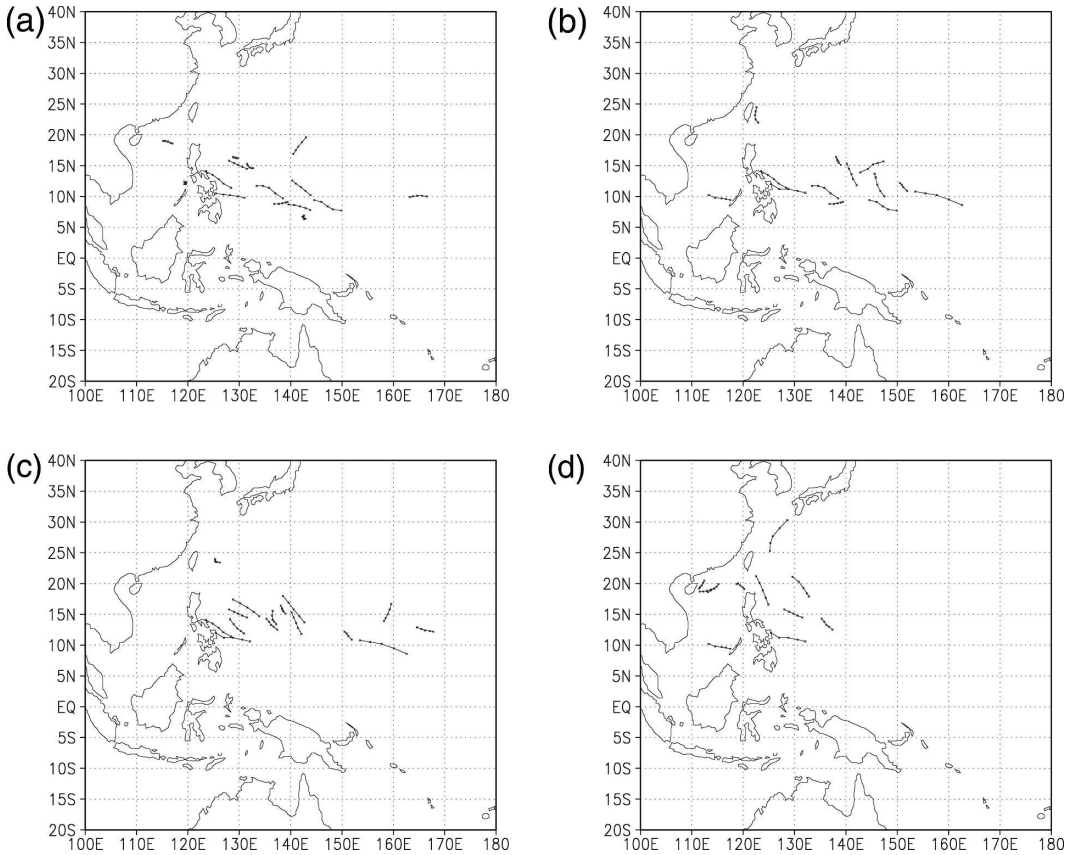

FIG. 13. (a)–(d) Track during RI for cases in Figs. 11a–d.

few hundred kilometers of the lower-level TC circulation prior to intensification. A similar approach to that of Hanley et al. (2001) is adopted in defining a so-called superposition case, in that the trough and lower-level TC center must approach to less then 500 km prior to intensification. Two case studies of RI are discussed here, one involving a TUTT and the other involving a midlatitude trough. A total composite of the 15 RI cases is compared to 7 SI cases. The results show a remarkable similarity to some Atlantic case studies.

a. Potential vorticity (PV) as a proxy for TC–trough interaction

Following Hoskins et al. (1985) and others, PV provides a more concise dynamical framework for examining TC–trough interactions. The added benefit of PV lies in its conservation properties in adiabatic and frictionless flow. Material changes in PV can be directly related to diabatic processes. In this study Ertel isentropic PV (IPV) is calculated at the 350-K level (about 200 mb). This level was chosen, as it was found to have the most clear and consistent signal in IPV evolution in the analyses, and is close to the level used in prior studies. IPV is defined by

$$\mathrm{IPV} = -g\frac{(\mathbf{s}_\theta + f)}{\partial p/\partial\theta}, \tag{1}$$

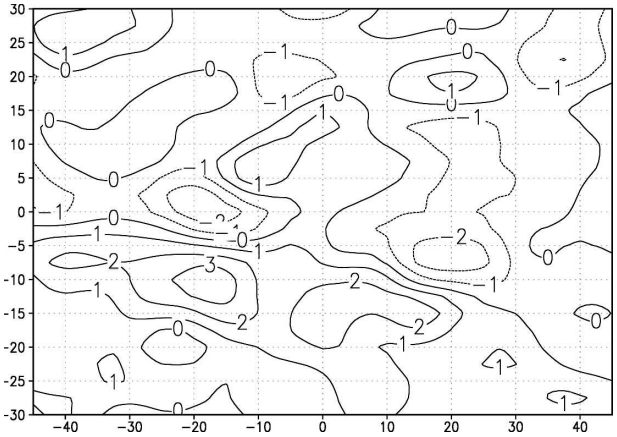

FIG. 14. Composite anomaly zonal wind ($\mathrm{m\,s^{-1}}$) at 850 mb for 19 cases of VRI from initial intensity of 35 kt. The x axis is the storm's relative longitude and the y axis is the storm's relative latitude.

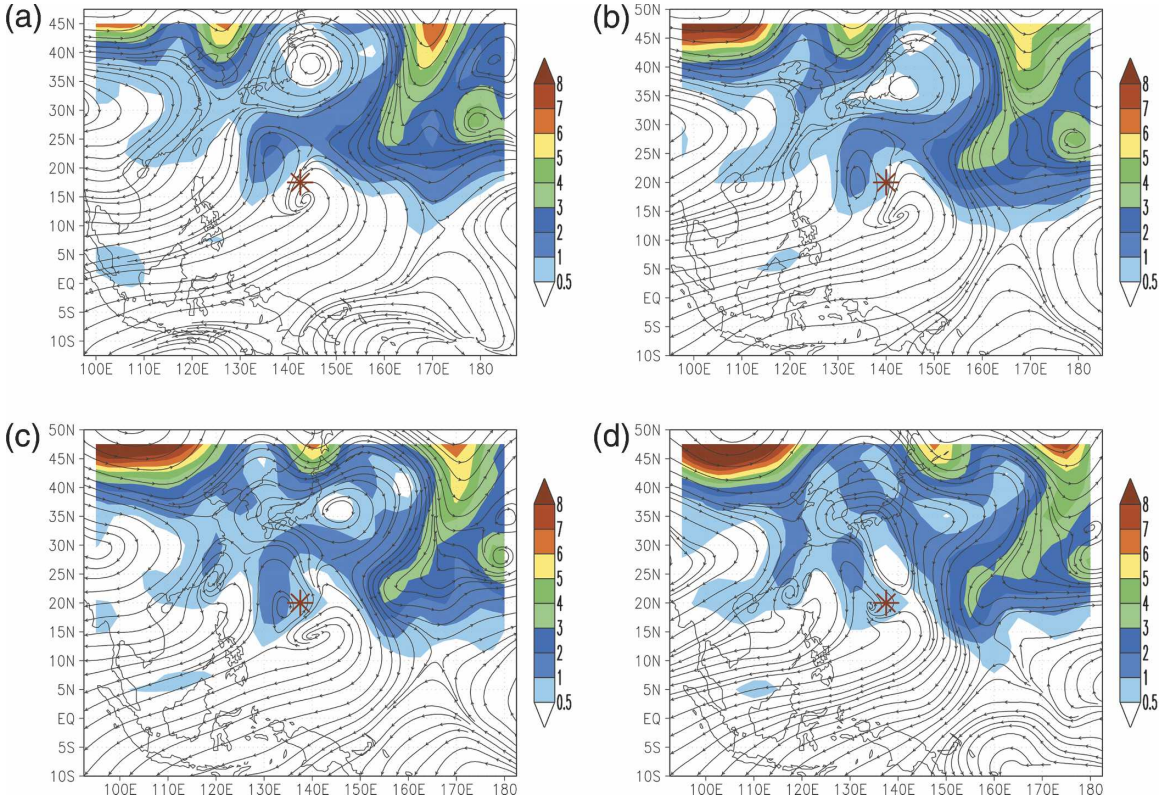

FIG. 15. The PV [shaded (PVU)] and streamlines at 350 K for TS Nelson (August 1985). Relative to onset of RI at (a) −24, (b) −12, (c) 0, and (d) +12 h. The stars mark the location of the surface tropical storm.

where g is the acceleration of gravity, $s_\theta + f$ is the absolute vorticity on an isentropic surface, p is air pressure, and θ is potential temperature. IPV describes the potential for vorticity creation by changing latitude [numerator of (1)] and/or adiabatically changing the separation of isentropic layers as represented by the denominator in (1). All variables involved in the calculation of IPV are linearly interpolated to θ coordinates and IPV will be expressed in the units of Hoskins et al. (1985) ($1\ \text{PVU} = 1 \times 10^{-6}\ \text{m}^2\ \text{K}\ \text{s}^{-1}\ \text{kg}^{-1}$).

b. Case study discussion

Tropical Storm Nelson (August 1985) was approached by a cutoff TUTT circulation prior to RI. Tropical Storm Nelson was located near 21°N, 140°E at the time of first reaching TS intensity. Figure 15 shows a horizontal cross section of the evolution of IPV at 350 K, 24 h (−24 h) before onset of RI, 12 h (−12 h) before, 0 h (0 h) and 12 h (+12 h) into RI. The positive IPV anomaly and TS approach between −24 and −12 h with high values of 1 PVU almost (but not) crossing the lower-level TS circulation at 0 h. As TS Nelson intensifies, the IPV anomaly weakens rapidly.

Figure 16 depicts the evolution of a vertical cross section of PV, this time on pressure surfaces. Isentropes are contoured for reference. The cross section is orientated in a northwest–southeast direction to best capture the approach of the PV anomaly to the northwest of the lower-level TS circulation. The stars mark the location of the TC circulation. The PV values in excess of 1.75 PVU extend downward to near 275 mb. The high values approach TS Nelson but never directly cross the storm. Marked weakening of the PV anomaly can be seen between 0 and +12 h, along with the development of high PV in the lower levels associated with the rapidly developing TS. Interestingly an intensifying PV maximum exists far to the east-southeast of TS Nelson.

Tropical Storm Vanessa developed in October of 1984 and satisfied the definition of RI. Prior to the intensification, the trailing end of an upper-level midlatitude trough dug south of 12°N, with TS Vanessa located at 9.4°N, 154.4°E after first reaching TS intensity. Figure 17 shows the evolution of IPV in horizontal cross sections at 350 K, with the same RI relative time periods as for TS Nelson (Fig. 15). Through the time series of events the midlatitude trough, whose main axis

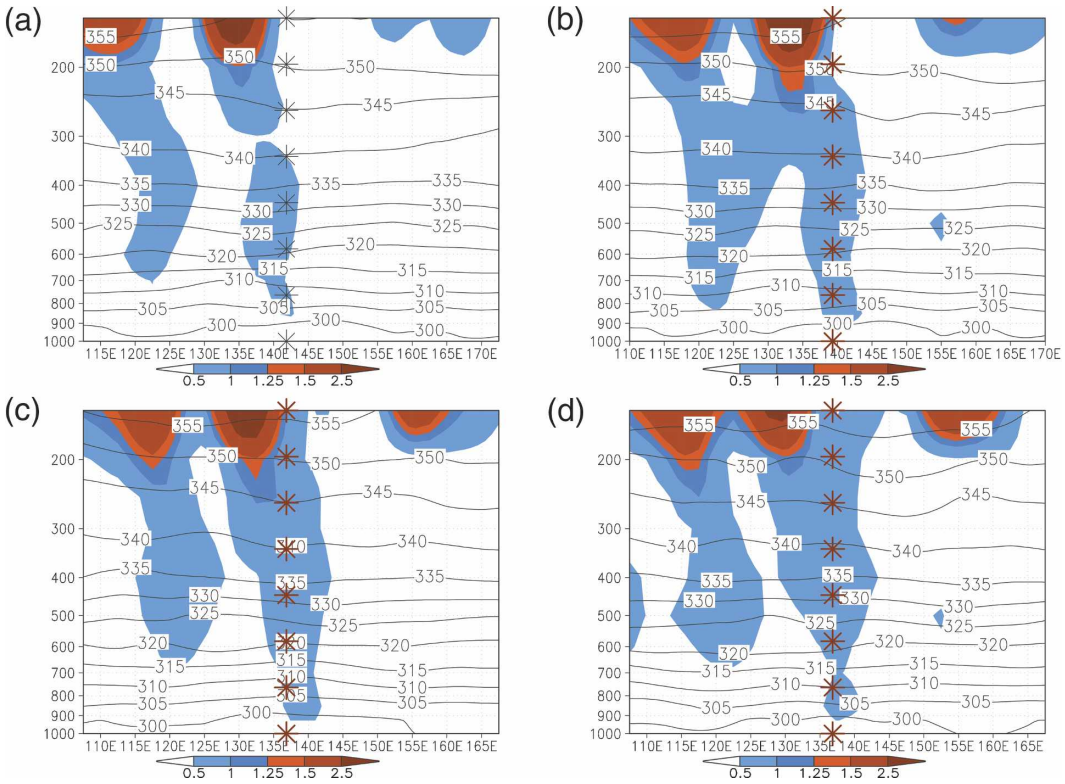

FIG. 16. Northwest–southeast vertical cross section through the upper-level trough and TS Nelson (1985). The PV (PVU units) is shaded and isentropes (K) are contoured. The stars mark the location of the tropical storm. Times are the same as in Fig. 15.

tilts in a northeast–southwest direction, moves slightly south of due east. Its trailing edge (as identified by positive IPV values) approaches between −24 and −12 h. At −12 h a PV maximum exceeding 1 PVU is within 300 km of the lower-level circulation. Over the next two time periods, as RI begins, the IPV maximum rapidly dissipates. This sequence of events, with only a small portion of the IPV anomaly approaching the TS, resembles the Molinari et al. (1995) picture of a trough interaction with Hurricane Elena. A strong midlatitude trough is always associated with strong vertical wind shear, which is well known to hinder or reverse TC intensification. In the case of Hurricane Elena and this study's case, only the base of the trough approaches, resulting in a modest increase of vertical wind shear (not shown). The destruction of the upper-level IPV anomaly is a symptom of the onset of RI. As the IPV anomaly gets close to the TC center it is annihilated by diabatic heating associated with condensation in updrafts near the TC center. The ability of the TC to destroy the IPV anomaly is thought to be important as this reduces the length of time any additional vertical wind shear may be over the center. The vertical cross section is not shown due to its similarity to TS Nelson (Fig. 15).

c. *Total composite PV evolution*

Figure 18 reveals the result of compositing all 15 cases for the same time periods relative to the onset of intensification as above. Between −24 and −12 h a lobe of high IPV air approaches within 500 km of the lower-level TC circulation. The 0.5-PVU contour actually crosses the TC center at −12 h. As intensification begins, the lobe of positive IPV weakens near the TS center. The character of events is similar to that of the case studies and gives further confidence to the repeatability of trough interaction prior to intensification. The Hanley et al. (2001) study shows a similar sequence of events in their Atlantic composite study. These cases are so-called positive superposition cases. Notable differences are that Hanley at al. (2001) used European Centre for Medium-Range Weather Forecasts (ECMWF) data and their storms were not limited to have a prescribed initial intensity. It follows to examine the slower intensifier set to investigate the similarity or difference in the character of TS–upper-level trough

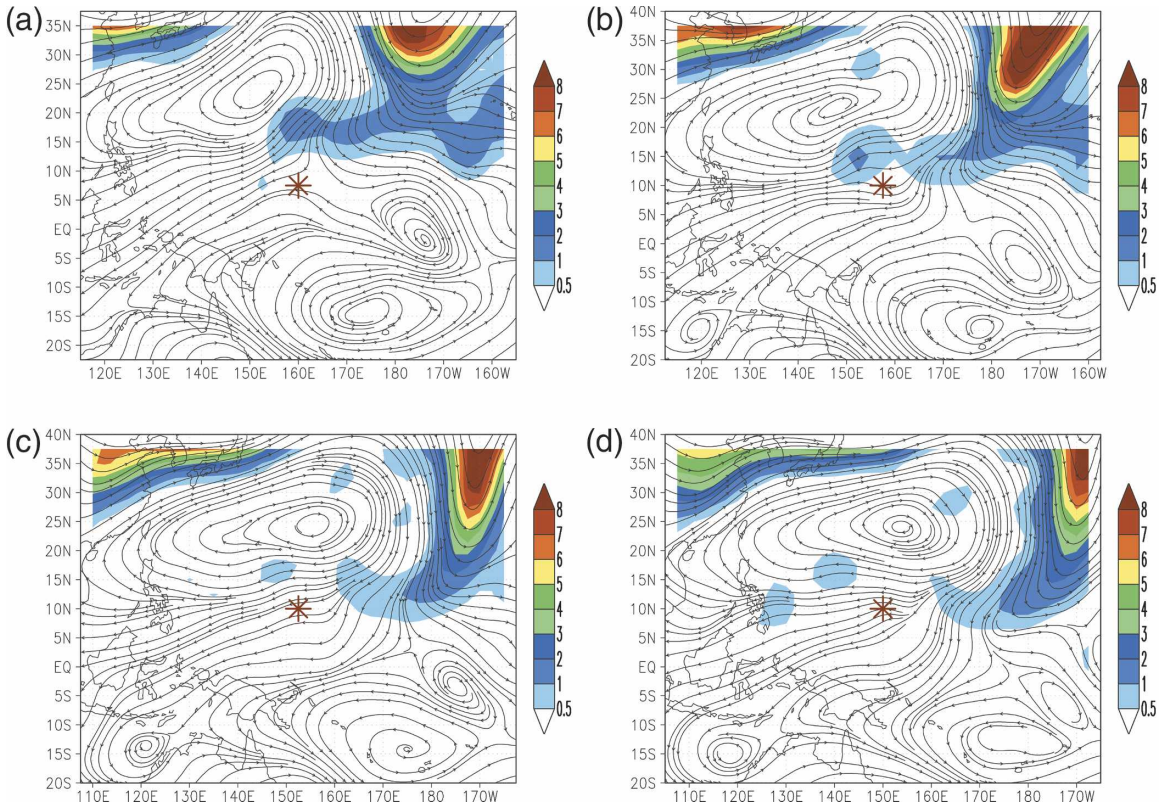

FIG. 17. The PV [shaded (PVU)] and streamlines at 350 K for TS Vanessa (October 1984). Relative to onset of RI at (a) −24, (b) −12, (c) 0, and (d) +12 h. The stars mark the location of the surface tropical storm.

interactions. Although these interactions will still be viewed as "positive," is there a difference that makes them less so?

d. SIs–upper-level trough interaction

The seven cases approached closely by upper-level troughs with resultant SI are presented in a composite sense (Fig. 19) over the same time frame as the RI cases. A similar yet subtly different sequence of events occurs. Again the composite TS is approached between $t - 24$ and $t + 0$, so that PVU > 1 comes within 500 km of the center of the TS. The main difference is that the PV anomaly lobe is broader than is the case for the RI composite picture (Fig. 18). The maximum IPV values associated with the trough at 350 K are slightly larger than for the RI case. The broadness and maximum IPV values of the upper-level lobe should be directly proportional to the vertical shear that it imparts. Indeed, looking at the composite difference of the vertical wind shear magnitude between the SI and RI cases at $t + 0$ (Fig. 20) shows that over the center of the trough, some 10° to the northwest, the vertical shear is over 6 m s^{-1} greater for the SI cases. Over the center of the TS there is a small increase of vertical shear (<2 m s^{-1}). The 200–850-mb shear computation near the center of the vortex should be approached with caution, since the circulation of the TS cannot be separated clearly from the environment. However, the broad area of stronger vertical wind shear associated with the SI composite trough gives confidence in the conclusion that there is indeed more vertical wind shear for the SI cases.

5. Conclusions and further research

A new definition of RI was defined based on the finding that the intensification rate is dependent on the initial intensity of WNP TCs. Composite and EOF analysis were employed using NCEP–NCAR reanalysis in conjunction with JTWC best-track data to find the character and repeatability of lower- and upper-level large-scale circulation patterns occurring just prior to RI from early TS stage. Composite analysis revealed the importance of outflow being less hindered to the north as well as south for RI cases at 200 mb. Using EOF analysis, clear preference for 850-mb anomalous confluence and combined confluence–horizontal shear patterns were found to occur prior to VRI from initial

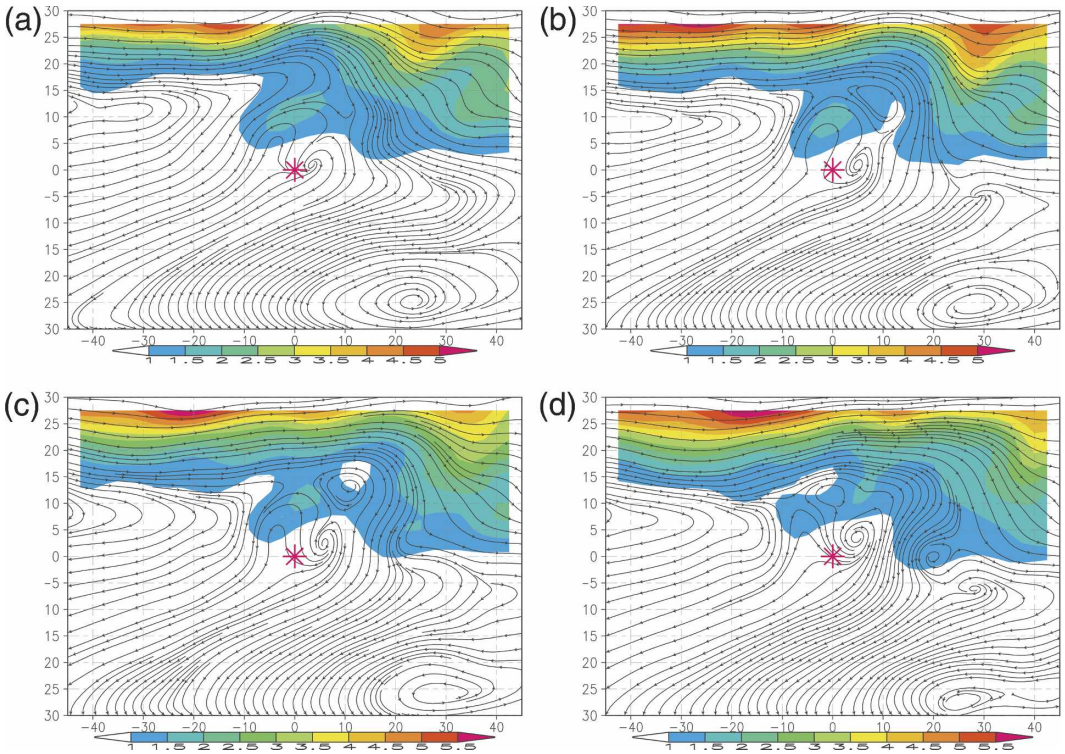

FIG. 18. Composite PV (shaded PVU units) and streamlines at 350 K for 15 RI cases. The time sequence relative to the onset of RI is the same as in Fig. 15.

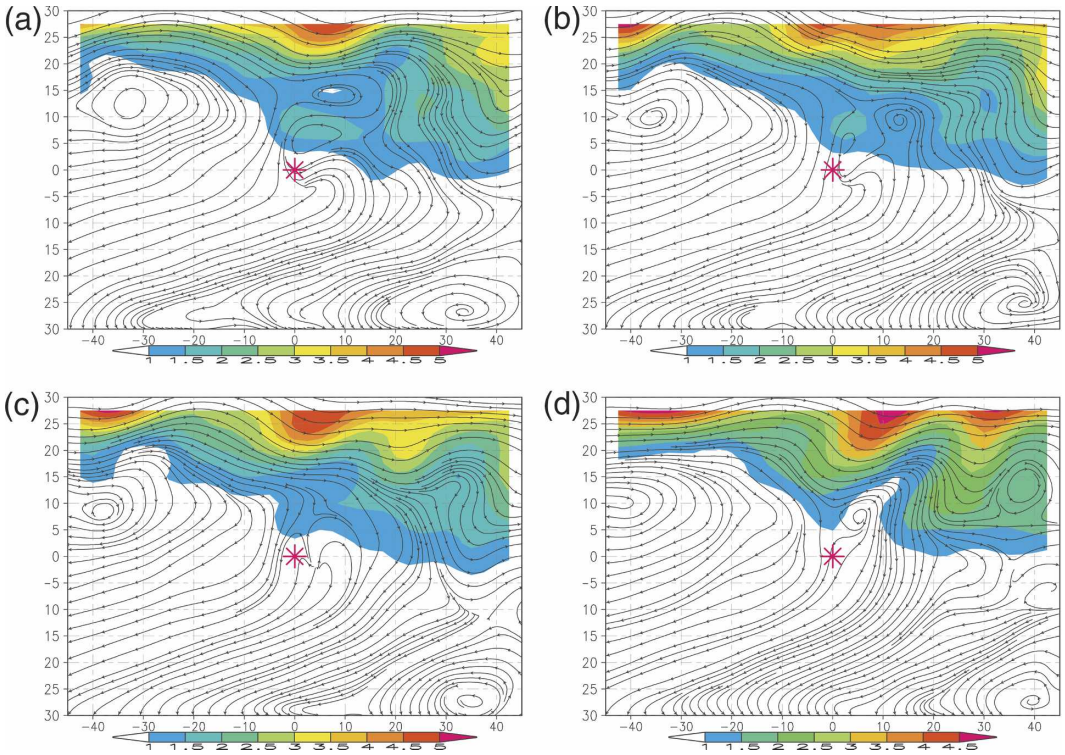

FIG. 19. Same as in Fig. 18, but for seven SI cases.

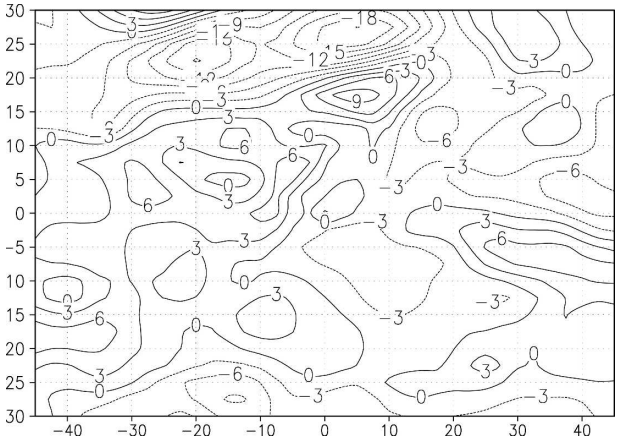

FIG. 20. Composite difference in the magnitude of the 200–850-mb vertical wind shear ($m\ s^{-1}$) for seven SI cases minus 15 RI cases at 0 h (onset of intensification). The *x* axis is the storm's relative longitude and the *y* axis is the storm's relative latitude.

35-kt intensity. VRI cases distinguish themselves in the character of the lower-level flow, whereas there is little difference between SI and RI cases. The clarity of this new result suggests there may be some forecast benefit from recognizing these characteristic low-level flow patterns.

The TS–trough interactions were also studied and the results were similar to prior Atlantic case studies. The similarity of individual case studies and the composite picture points to a repeatable physical event prior to RI involving upper-level troughs. A small-scale PV anomaly and TS mutually approach just prior to the onset of RI. The PV anomaly's main bulk never actually crosses the center of the TS as is it weak enough that TS convection and associated diabatic heating effectively kills the cold core anomaly, before any great increase in vertical shear is able to negatively affect the TS. For SI cases the troughs are stronger and broader leading to more vertical shear in the environment (6 $m\ s^{-1}$ maximum) and over the TS (2 $m\ s^{-1}$ more). It seems reasonable that vertical shear is the deciding factor as to how favorable or unfavorable an interaction will be. The precise mechanism of intensification remains to be explored. Positive superposition and interference of an upper- and lower-level PV anomaly leading to an enhanced in, up, and out circulation of the TS and resultant intensification by increased surface fluxes remain a possible candidate. Until this is more clearly demonstrated, at least it may be possible to derive some operational forecast benefit from the Hanley et al. (2001) work and the results of this study, rather than a complete physical understanding.

It is difficult to determine physically why the lower-level flow pattern described is more favorable for VRI from the analyses presented. The strong confluence patterns and upper-level TUTT systems to the east of the TS appear to be a coupled system. The addition of the TUTT in such a location may enhance the confluence pattern below by increasing subsidence on the TUTT's western side, strengthening the subtropical ridge below and its attendant trade winds. Nevertheless, the clarity and the repeatability of the signal for the VRI cases deserve further investigation *as an additional RI predictor*. A modeling study on the effects of horizontal shear and environmental flow convergence on TC structure and intensity is currently under way (Ventham 2005), in an effort to provide more concrete physical mechanisms based on the results of this study.

Acknowledgments. This research was supported by the U.S. Office of Naval Research under Grant N00014-021-0532. This work comprises part of a Ph.D. dissertation, and thanks go to the dissertation committee for their valuable input. The authors thank two anonymous reviewers for their useful suggestions and criticisms.

REFERENCES

Bender, M. A., 1997: The effect of relative flow on the asymmetric structure of the interior of hurricanes. *J. Atmos. Sci.,* **54,** 703–724.

Chen, L. S., and W. M. Gray, 1985: Global view of the upper level outflow patterns associated with tropical cyclone intensity changes during FGGE. Department of Atmospheric Science Paper 392, Colorado State University, Ft. Collins, CO, 126 pp.

DeMaria, M., 1996: The effect of vertical shear on tropical cyclone intensity change. *J. Atmos. Sci.,* **53,** 2076–2087.

Hanley, D., J. Molinari, and D. Keyser, 2001: A composite study of the interactions between tropical cyclones and upper-tropospheric troughs. *Mon. Wea. Rev.,* **129,** 2570–2584.

Holliday, C. R., and A. H. Thompson, 1979: Climatological characteristics of rapidly intensifying typhoons. *Mon. Wea. Rev.,* **107,** 1022–1034.

Hoskins, B. J., M. E. McIntyre, and A. W. Robertson, 1985: On the use and significance of isentropic potential vorticity maps. *Quart. J. Roy. Meteor. Soc.,* **111,** 877–946.

Kaplan, J., and M. DeMaria, 2003: Large-scale characteristics of rapidly intensifying tropical cyclones in the North Atlantic basin. *Wea. Forecasting,* **18,** 1093–1108.

Mallen, K. J., M. T. Montgomery, and B. Wang, 2005: Reexamining tropical cyclone near-core radial structure using aircraft observations: Implications for vortex resiliency. *J. Atmos. Sci.,* **62,** 408–425.

Molinari, J., S. Skubis, and D. Vollaro, 1995: External influences on hurricane intensity. Part III: Potential vorticity structure. *J. Atmos. Sci.,* **52,** 3593–3606.

Mundell, D. B., 1990: Prediction of tropical cyclone rapid intensification events. AFIT/CI/CIA-90-104, M.S. thesis, Dept. of Atmospheric Science, Colorado State University, Fort Collins, CO, 186 pp.

North, G. R., T. L. Bell, R. F. Cahalan, and F. J. Moeng, 1982: Sampling errors in the estimation of empirical orthogonal functions. *Mon. Wea. Rev.,* **110,** 699–706.

Peak, J. E., W. E. Wilson, R. L. Elsberry, and J. C.-L. Chan, 1986: Forecasting tropical cyclone motion using empirical orthogonal function representations of the environmental wind fields. *Mon. Wea. Rev.,* **114,** 2466–2477.

Ritchie, E. A., and G. J. Holland, 1999: Large-scale patterns associated with tropical cyclogenesis in the western Pacific. *Mon. Wea. Rev.,* **127,** 2027–2043.

Sadler, J. C., 1975: *The Upper Tropospheric Circulation over the Global Tropics.* Dept. of Meteorology, Atlas UHMET 75-05, University of Hawaii at Manoa, Honolulu, HI, 35 pp.

Spratt, S. C., 1990: Tropical cyclone cloud patterns: Climatology and relationship to intensity changes. M.S. thesis, University of Hawaii at Manoa, Honolulu, HI, 108 pp.

Titley, D. W., and R. L. Elsberry, 2000: On rapid intensity changes in tropical cyclones: A case study of Supertyphoon Flo during TCM-90. *Mon. Wea. Rev.,* **128,** 3556–3573.

Ventham, J. D., 2005: Large scale environmental wind patterns and the intensification rates of western North Pacific tropical storms. Ph.D. dissertation, University of Hawaii at Manoa, Honolulu, HI, 212 pp.